

The Tokyo Axion Helioscope

R. Ohta^{a,*}, Y. Akimoto^b, Y. Inoue^{c,h}, M. Minowa^{a,h}, T. Mizumoto^d, S. Moriyama^e, T. Namba^c, Y. Takasu^f, A. Yamamoto^{g,h}

^a*Department of Physics, School of Science, University of Tokyo, 7-3-1 Hongo, Bunkyo-ku, Tokyo 113-0033, Japan*

^b*School of Science, University of Tokyo, 7-3-1 Hongo, Bunkyo-ku, Tokyo 113-0033, Japan*

^c*International Center for Elementary Particle Physics, University of Tokyo, 7-3-1 Hongo, Bunkyo-ku, Tokyo 113-0033, Japan*

^d*Department of Physics, Graduate School of Science, Kyoto University, Kitashirakawa-oiwake-cho, Sakyo-ku, Kyoto 606-8502, Japan*

^e*Institute for Cosmic Ray Research, University of Tokyo, 456 Higashi-Mozumi, Kamioka-cho, Hida, Gifu 506-1205, Japan*

^f*Tsukuba, Ibaraki, Japan*

^g*High Energy Accelerator Research Organization, 1-1 Oho, Tsukuba, Ibaraki 305-0801, Japan*

^h*Research Center for the Early Universe (RESCEU), School of Science, University of Tokyo, 7-3-1 Hongo, Bunkyo-ku, Tokyo 113-0033, Japan*

Abstract

The Tokyo Axion Helioscope experiment aims to detect axions which are produced in the solar core. The helioscope uses a strong magnetic field in order to convert axions into X-ray photons and has a mounting to follow the sun very accurately. The photons are detected by an X-ray detector which is made of 16 PIN-photodiodes. In addition, a gas container and a gas regulation system is adopted for recovering the coherence between axions and photons in the conversion region giving sensitivity to axions with masses up to 2 eV. In this paper, we report on the technical detail of the Tokyo Axion Helioscope.

Keywords: solar axion, helioscope, PIN photodiode, superconducting magnet

1. Introduction

Axions are light neutral pseudoscalar particles which are introduced to solve the strong CP problem [1]. They would be produced in the solar core via the Primakoff conversion of the plasma photons if they have large enough coupling to photons [2] [3]. The Tokyo Axion Helioscope experiment (also known as

*Corresponding author.

Email address: comic@icepp.s.u-tokyo.ac.jp (R. Ohta)
Preprint submitted to Nuclear Instruments and Methods in Physics Research A August 23, 2018

25 Sumico experiment) aims to detect solar axions by tracking the sun (Fig. 1).
 26 The helioscope consists of a tracking system, a superconducting magnet, a gas



Figure 1: Photograph of Tokyo Axion Helioscope

27 regulation system, and an X-ray detector. The magnet, the gas container and
 28 the X-ray detector are assembled in a 3-m long cylinder. The tracking system
 29 supports and drives the cylinder of the helioscope to align the helioscope axis
 30 with the direction of the sun.

Axions are converted into photons with energy of several keV, reflecting
 temperature of the solar core. These photons are detected by an X-ray detector.
 The detection principle is based on the coupling of an incoming axion to a virtual
 photon provided by the transverse magnetic field of an intense dipole magnet.
 Thus the incoming axion is converted into a real, detectable photon that carries
 the energy of the original axion. The conversion rate is given by [3]

$$P_{a \rightarrow \gamma} = \left| \frac{g_{a\gamma\gamma}}{2} \exp \left[- \int_0^L dz \Gamma/2 \right] \times \int_0^L dz B_{\perp} \exp \left[i \int_0^z dz' \left(q - \frac{i\Gamma}{2} \right) \right] \right|^2, \quad (1)$$

31 where $g_{a\gamma\gamma}$ is the coupling constant between axions and photons, z and z' are

32 the coordinate along the incoming axion, B_{\perp} is the strength of the transverse
 33 magnetic field, L is the length of the field along z -axis, Γ is the X-ray absorption
 34 coefficient of medium with which the conversion region is filled, $q = (m_{\gamma}^2 -$
 35 $m_a^2)/2E$ is the momentum transfer by the virtual photon, and m_{γ} is the effective
 36 mass of the photon which equals to zero in vacuum.

37 Axions have not been discovered yet in any of the past experiments. In
 38 the first phase [4] of our experiment, the conversion region was vacuum and
 39 the experimental limit is given to be $g_{a\gamma\gamma} < 6.0 \times 10^{-10} \text{ GeV}^{-1}$ (95% C.L.) for
 40 $m_a < 0.03 \text{ eV}$. To detect heavy axions, the momentum transfer should be kept
 41 negligible by introducing a dispersion matching medium into the conversion
 42 region. For this purpose, helium gas was used in the second phase [5] and the
 43 limit is given to be $g_{a\gamma\gamma} < 6.3 - 10.5 \times 10^{-10} \text{ GeV}^{-1}$ (95% C.L.) for $m_a < 0.27 \text{ eV}$.
 44 The third phase [6] was also performed using denser helium gas than that of the
 45 second one and the limit is given to be $g_{a\gamma\gamma} < 5.6 - 13.4 \times 10^{-10} \text{ GeV}^{-1}$ (95%
 46 C.L.) for $0.84 < m_a < 1.00 \text{ eV}$.

47 In this paper, we report on the technical detail of the Tokyo Axion Helio-
 48 scope.

49 2. Tracking System

50 The tracking system consists of a driving mechanism, direction measuring
 51 encoders and a PC (computer 1). They form a feedback control loop as a whole.
 52 A schematic view of the driving system is shown in Fig. 2. We adopted an
 53 altazimuth mount as the driving mechanism. The altazimuth mount minimizes
 54 inclination of the refrigerator and can support the magnet with simple structure.
 55 The driving mechanism is composed of an axle bearing, a turntable, a ball screw,
 56 and two AC servomotors. The cylinder is supported by the axle bearing on the
 57 turntable. In the azimuthal direction, the turntable is driven by one of the
 58 servomotors (Hitachi EPS8). In the altitudinal direction, the cylinder is driven
 59 by the other servomotor (Hitachi EPL3TD) through the ball screw.

60 The axion helioscope is located in Tokyo at $139^{\circ}45'48''\text{E}$ and $35^{\circ}42'49''\text{N}$.

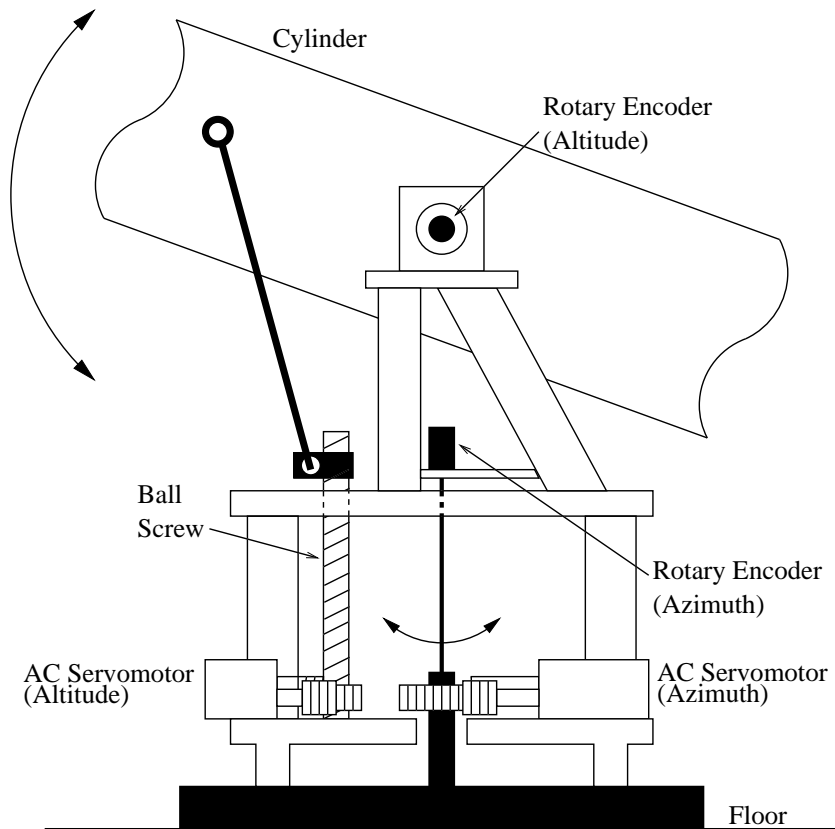


Figure 2: Schematic view of driving system

61 In usual operation, the driving range of the helioscope is from -28° to 28° in
 62 the altitudinal direction and the range of the azimuthal direction is 360° . Its
 63 azimuthal direction is limited only by a limiter which prevents the helioscope
 64 from endless rotation. Within this limitations, the helioscope can track the Sun
 65 half of a day averagely.

66 The control diagram of the tracking system is shown in Fig. 3. The driving
 67 mechanism is wholly controlled by computer 1 via CAMAC bus.

68 The azimuthal and altitudinal directions of the helioscope are measured by
 69 two precision rotary encoders (Canon R-1 L) each of which produces 81,000
 70 pulse-per-revolution quadrature outputs in A and B channels and a zero index

71 output in Z channel to indicate its angular origin. The encoder pulses are sent
72 to a homemade pulse counter by which computer 1 obtains the absolute angle
73 of each encoders with a resolution of 1/324,000 revolution or 4 arcseconds (ca.
74 $19 \mu\text{rad}$).

75 Each AC servomotor is controlled through a homemade CAMAC pulse gener-
76 erator. Every 0.2 second, computer 1 calculates the amount and the frequency
77 of the pulses, namely the angle and the speed of rotation, for the next period
78 based on the measured- and targeted directions of the helioscope.

79 The overall tracking accuracy is better than 0.5 mrad both in altitudinal and
80 azimuthal direction. Main components of the errors are the fluctuation of the
81 turntable and the misalignment of the magnet aperture and the helioscope axis.

82 The guidance of the helioscope movement is provided by the tracking soft-
83 ware. In order to calculate the position of the sun, the U. S. Naval Observa-
84 tory Vector Astronomy Subroutines (NOVAS-C ver 2.0.1) [7] is used. NOVAS-
85 C calculates the topocentric position of the sun with less than 2 arcseconds
86 ($= 9.7 \mu\text{rad}$) error which is negligible in our measurements.

87 **3. Superconducting Magnet**

88 Incoming solar axions are converted into photons by magnetic field of the
89 superconducting magnet. The conversion efficiency of axions depends strongly
90 on the strength and length of the magnetic field as shown in Eq.(1).

91 Two devices make it easy to swing the magnet. Firstly, the magnet is made
92 cryogen-free by using two Gifford-McMahon refrigerators (GM refrigerators).
93 Therefore, no liquid helium tube is needed. Secondly, a persistent current switch
94 (PCS) is equipped and the magnet is free from thick current leads.

95 *3.1. Magnet and Cryogenics*

96 The superconducting magnet consists of two 2.3-m long race-track shaped
97 coils running parallel with a 20-mm wide gap between them. In this gap, the
98 gas container is inserted and axions are converted into photons, which are to

99 be detected by the X-ray detector. A schematic view of the magnet is shown in
100 Fig. 4.

101 The coils are made of copper-clad NbTi superconducting wires and housed
102 in a stainless steel case. They are kept at 5–6 K during operation. The magnetic
103 field in the gap is about 4 T perpendicular to the helioscope axis when a current
104 is 268 A. The magnet is cooled by two GM refrigerators each of which is two
105 staged. The radiation shield of the cryostat is connected with the first-stage cold
106 heads where the temperature reaches about 40 K in normal operation. The coils
107 are connected with the second stage, which reaches about 4 K, through a ther-
108 mal conductive rod and plates made of oxygen-free high-conductivity (OFHC)
109 copper. High- T_c superconducting current leads are used between the first and
110 the second stages.

111 Thermometers are attached to the coils, cold heads of refrigerators etc. to
112 measure the temperature distribution. As thermometers, Carbon Glass Resis-
113 tors (CGRs) and platinum-cobalt resistors (PtCos) are used. CGRs are used to
114 measure low temperatures (5–10 K) and PtCos are sensitive at relatively high
115 temperatures (10–300 K). Each CGR was calibrated by the manufacturer. Two
116 Hall sensors are also attached to the coils to measure the strength of the mag-
117 netic field.

118 *3.2. Persistent Current Switch*

119 The magnet can be operated in persistent current mode by short-circuiting
120 the coils with the persistent current switch (PCS) [8]. In Fig. 5, a circuit
121 diagram of the magnet is shown. In this mode, the power supply is no longer
122 needed to maintain the magnetic field and the current leads can be disconnected
123 completely.

124 The PCS is mounted on a copper plate which is weakly coupled to the sec-
125 ond stage of the refrigerators. The PCS is made of superconducting wire and
126 an integrated heater to change its phase to normal phase. Before exciting the
127 magnet, the heater is switched on and keeps the temperature of the PCS above
128 9 K, which is the phase-transition temperature of the wire used in the PCS. The

129 PCS in normal phase has resistance around $11\ \Omega$. Then a magnet excitation
 130 starts with supplying current. When the current reaches the final value, excita-
 131 tion voltage goes to zero and the heater is switched off to cool the PCS down.
 132 After the PCS goes back to superconducting phase, the supplying current can
 133 be decreased to zero while the current in the main circuit is maintained.

134 4. Gas Regulation System

135 4.1. Coherence between Axion and Photon

136 To keep coherence between axion and photon, m_γ has to be tuned to m_a by
 137 introducing gas into the conversion region. For this purpose, the gas container
 138 is inserted into the aperture of the magnet.

A photon in the X-ray region acquires a positive effective mass in a medium.
 It is well approximated by

$$m_\gamma = \sqrt{\frac{4\pi\alpha N_e}{m_e}} \quad (2)$$

139 as for the light gas, such as hydrogen or helium, where α is the fine structure
 140 constant, m_e is the electron mass, and N_e is the number density of electrons [3].
 141 Cold helium gas was adopted as a dispersion matching medium, because helium
 142 gas has small X-ray absorption length and remains at gas state at 5 K, the
 143 operating temperature of our magnet, at 1 atm. If m_a differs from m_γ , coherence
 144 between axion and photon is lost and the conversion efficiency decreases. From
 145 Eq. (1), the condition in which the conversion efficiency has significant value is
 146 $qL \lesssim \pi$. For a given effective mass, axion masses m_a within a very narrow range
 147 satisfy this condition. The width of this window is about 2 meV (FWHM) at
 148 $m_\gamma \simeq 1$ eV. To sweep the axion mass range up to a few eV, we need to change
 149 the gas density more than a thousand times. To control the gas density, we
 150 need to control the pressure accurately and to keep the temperature constant.
 151 Therefore we developed an automatic pressure and temperature control system
 152 of helium gas in the gas container for the third phase of solar axion search [6].

153 *4.2. Gas Container*

154 The body of the container is made of four 2.3-m long 0.8-mm thick stainless-
155 steel rectangle pipes welded side by side to each other. The entire body is
156 wrapped with 5N high purity aluminum sheet to achieve high uniformity of
157 temperature. The measured thermal conductance between the both ends was
158 1×10^{-2} W/K at 6K when the magnetic field is 4T. One end at the forward
159 side of the container is sealed with welded plugs and is suspended firmly by
160 three Kevlar cords, so that thermal flow through this end is highly suppressed.
161 The opposite side nearer to the X-ray detectors is flanged and fixed to the
162 magnet. At this end of the container, gas is separated from vacuum with an
163 X-ray window (Fig. 6) manufactured by METOREX which is transparent to X-
164 ray above 2keV and can hold gas up to 0.3MPa at liquid helium temperature.
165 The window is composed of 25- μ m thick Be foils, 1.5- μ m Ni support grids and
166 Ni frames. The foils have 1- μ m polyimide coat on the one side. Though He gas
167 at 6 K and 0.3 MPa corresponds to the effective mass of about 4 eV, absorption
168 of the gas becomes dominant and sensitivity of the apparatus decreases in this
169 mass region.

170 *4.3. Pressure Control System*

171 To change effective mass of photon in the gas container, we developed the
172 pressure control system of which diagram is shown in Fig. 7. Main compo-
173 nents of this system are the gas container, a precision pressure gauge (YOKO-
174 GAWA MU101-AH1N), a helium gas bottle for providing gas, a diaphragm
175 pump (Pfeiffer Vacuum MVP 015-4) for suction, PCs for automatic regulation,
176 and three piezo-valves (HORIBA STEC PV-1000 series). The helium gas is
177 injected through PV1 and is sucked by the vacuum pump through PV2 or PV3.
178 The gas pressure is regulated by changing the gas flows through the piezo-valves
179 which are controlled by their control voltages. Two PV-1101 piezo-valves are
180 used in PV1 and PV2, while a PV-1302 is used in PV3. PV3 is used to reach
181 lower pressures below 10kPa, where the suction is not enough only with PV2.

182 The gas flow of a PV-1302 is 30 times as high as a PV-1101. Control volt-
183 ages are supplied by computer 2 through a digital to analog converter (Interface
184 PCI-3521).

185 In the third phase of this experiment, mass scanning was performed changing
186 the effective mass by decreasing the pressure step by step. In fact, PV1 was
187 opened only at the early stages of the scan until the gas pressure reached the
188 highest value p_s^{\max} , and was closed during the automatic-control sequences. The
189 automated sequences worked as follows:

- 190 • While the measured pressure p_m was higher than the set pressure of a
191 period p_s , PV2 (or PV3) was opened proportionally to $\Delta p = p_m - p_s$
192 as far as the flow rate was within the capability of the value. For larger
193 Δp , PV2 (or PV3) was fully opened. The coefficient was determined
194 empirically.
- 195 • Once p_m became less than p_s , PV2 (or PV3) was closed and remained
196 closed during measurement.
- 197 • When a measurement had finished, p_s was set to the next value and a new
198 sequence was repeated.

199 4.4. Temperature Control System

200 Because the gas container is fixed on the magnet which is thermally coupled
201 to the GM refrigerators, the temperature of the gas container is affected by fluc-
202 tuations of the cooling power of the refrigerators. We developed a temperature
203 control system, since it is crucial to keep the gas temperature constant to retain
204 density uniformity of the gas as well as to control its density reliably.

205 The diagram of the temperature control system is shown in Fig. 8. The
206 main components of this system are a heater and a CGR thermometer T5. T5
207 is measuring the temperature of a copper plate which is tightly joined with the
208 gas container. The heater is attached to the heat link between the copper plate
209 and the magnet. The current through the heater is controlled to keep the T5

210 temperature constant, where PI (Proportional-Integral) control is adopted. The
211 PI parameters are decided empirically.

212 **5. X-ray detector**

213 *5.1. PIN Photodiode X-ray Detector*

214 The X-ray detector to detect photons originating from axions consists of 16
215 PIN photodiodes, Hamamatsu Photonics S3590-06-SPL(Fig. 9), and 16 pream-
216 plifiers which amplify signals from the PIN photodiodes.

217 Each of preamplifiers is separated into two part called head and back-end
218 part. The head parts are mounted next to the photodiodes and include the
219 first stage FETs, feedback resistors, test pulse inputs and HV buffers. The
220 PIN photodiodes and the head parts are assembled in the helioscope cylinder.
221 The remaining circuits are placed out of the cylinder. The details of this X-ray
222 detector is described elsewhere [9] [10].

223 *5.2. Data Acquisition System*

224 The output signals of the preamplifiers are stored and analyzed so that we
225 will obtain energy spectrum of the signals. The data acquisition system is shown
226 in Fig. 10.

227 Firstly, signals from preamplifiers are filtered and low frequency components
228 are reduced. Since the cut off frequency of this filter is 3 kHz, it does not affect
229 X-ray signals whose rise time is 0.8–1.3 μ s but reduce microphonic noise. Next,
230 the filtered signal is amplified by a linear amplifier called the booster with a
231 gain of about 300 to fit the input range of the FADCs. These filter and booster
232 are mounted just beside the back-end parts of the preamplifiers.

233 After the booster, signals are sent to the FADCs (REPIC RPC-081) via 15-
234 m coaxial cables. The sampling period of the FADC is 0.1 μ s, the resolution is
235 8 bit, and the buffer depth is 1024 words. The FADCs are stopped 50 μ s after
236 the trigger signal is latched in the input registers (HOSHIN C005). The trigger
237 is made from a discriminator (Technoland N-TM405) and a shaping amplifier

238 (Clear-Pulse 4026) whose shaping time is $3\mu\text{s}$. When the FADC is stopped by
239 trigger, the input register tell the trigger to computer 1 and it takes waveform
240 from the FADCs via CAMAC bus. At the same time the livetime counter
241 is stopped. Because deadtime of each transfer is about 0.35s and cannot be
242 ignored in the measurement, the livetime is counted in millisecond accuracy by
243 a 1-kHz clock. This accuracy is needed to compare the solar tracking event and
244 the non-tracking event.

245 **6. Summary**

246 We developed the axion helioscope which aims to detect solar axions. This
247 experimental apparatus consists of the tracking system, the superconducting
248 magnet, the gas regulation system, and the X-ray detector. The tracking sys-
249 tem directs the main cylinder towards the sun. The magnet converts incoming
250 axions into photons and the unmanned gas regulation system enables us to
251 convert axions with masses up to eV scale. The X-ray detector measures con-
252 version photons and the DAQ system records the signal of the photons into the
253 computer. Using this apparatus, we have performed solar axion searches with
254 axion's mass up to 0.27 eV [4] [5] and around 1 eV [6]. Since we did not detect
255 an evident signal of axion, we are going to perform more massive solar axion
256 search with mass up to about 2 eV in the near future.

257 **7. Acknowledgements**

258 The authors thank the former director general of KEK, Professor H. Sug-
259 awara, for his support in the beginning of the helioscope experiment. This re-
260 search was partially supported by Grant-in-Aid for COE Research, the Japanese
261 Ministry of Education, Science, Sports and Culture (MEXT) and Grant-in-Aid
262 for Scientific Research (B), Japan Society for the Promotion of Science and also
263 by the Matsuo Foundation. Additional support was provided by Global COE
264 Program "Physical Sciences Frontier", MEXT, Japan.

265 **References**

- 266 [1] R. D. Peccei, H. R. Quinn, Phys. Rev. Lett. 38 (1977) 1440; R. D. Peccei,
267 H. R. Quinn, Phys. Rev. D 16 (1977) 1791.
- 268 [2] P. Sikivie, Phys. Rev. Lett. 51 (1983) 1415.
- 269 [3] K. van Bibber, P. M. McIntyre, D. E. Morris, G. G. Raffelt, Phys. Rev. D
270 39 (1989) 2089.
- 271 [4] S. Moriyama, M. Minowa, Y. Inoue, T. Namba, Y. Takasu, A. Yamamoto,
272 Phys. Lett. B 434 (1998) 147.
- 273 [5] Y. Inoue, T. Namba, S. Moriyama, M. Minowa, Y. Takasu, T. Horiuchi, A.
274 Yamamoto, Phys. Lett. B 536 (2002) 18.
- 275 [6] Y. Inoue, Y. Akimoto, R. Ohta, T. Mizumoto, A. Yamamoto, M. Minowa,
276 Phys. Lett. B 668 (2008) 93.
- 277 [7] G. H. Kaplan, et al., Astronomical Journal 97 (1989) 1197.
- 278 [8] S. Mizumaki, Ph. D thesis, “Study of the property of current propagation
279 about superconductive junction”, The Graduate University for Advanced
280 Studies, Mar. 1997.
- 281 [9] T. Namba, Y. Inoue, S. Moriyama, M. Minowa, Nucl. Instr. and Meth. A
282 489 (2002) 224.
- 283 [10] Y. Akimoto, Y. Inoue, M. Minowa, Nucl. Instr. and Meth. A 557 (2006)
284 684.

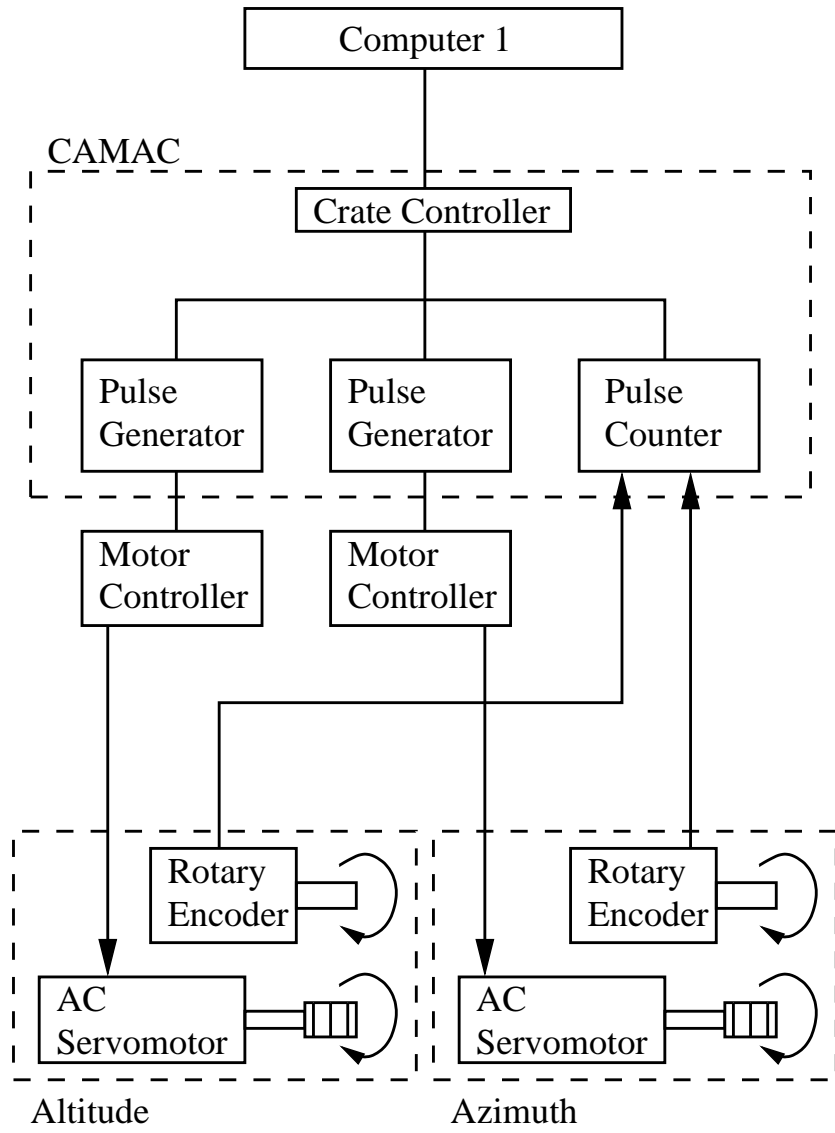


Figure 3: Control diagram of tracking system

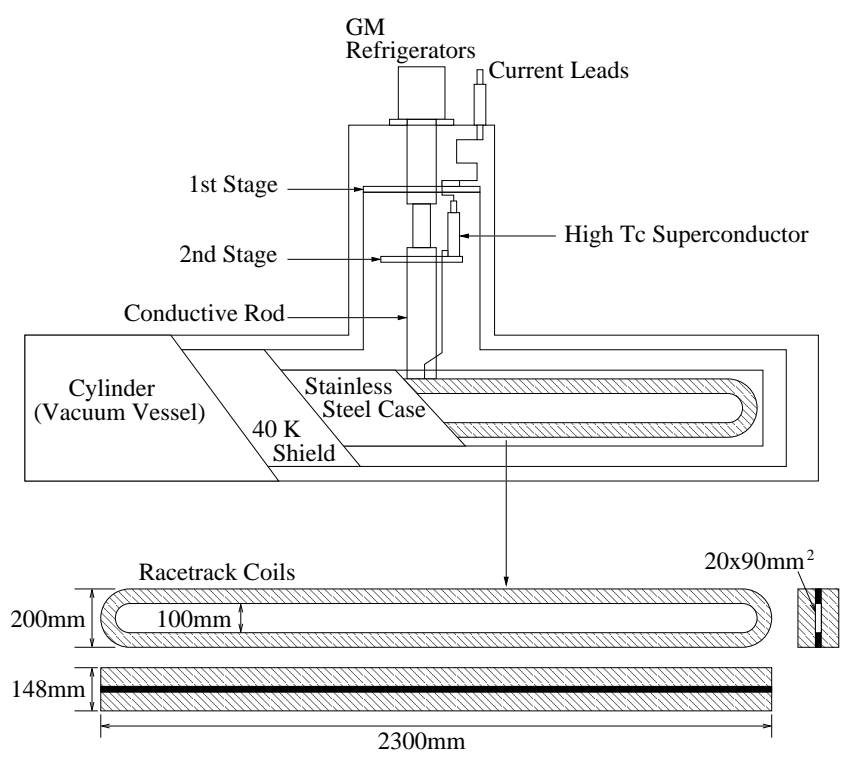


Figure 4: Schematic shape of race-track coils

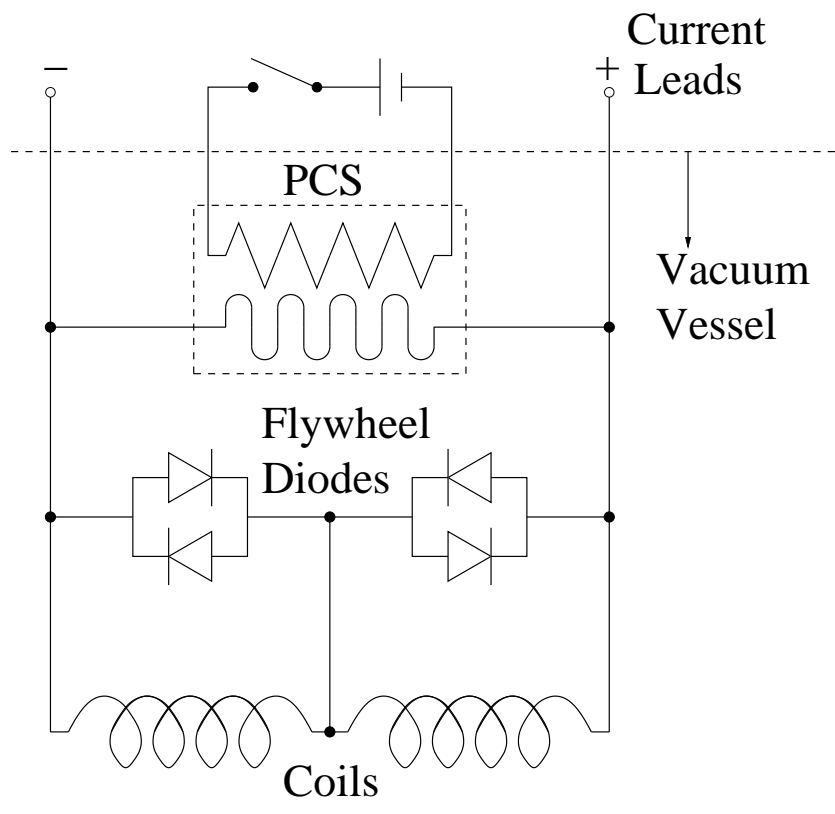


Figure 5: Circuit diagram of the magnet

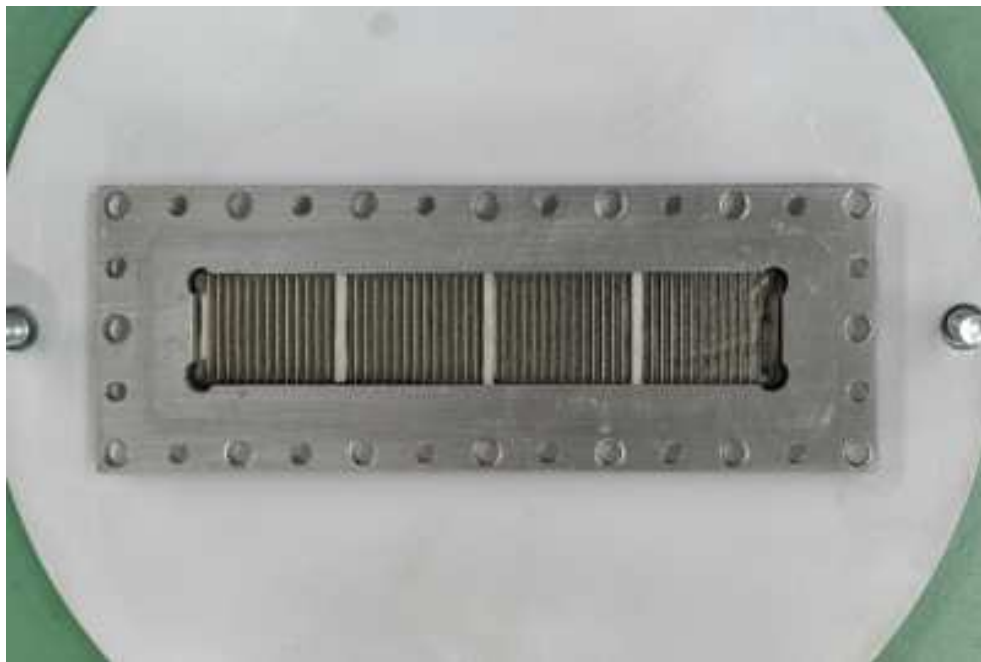


Figure 6: X-ray window

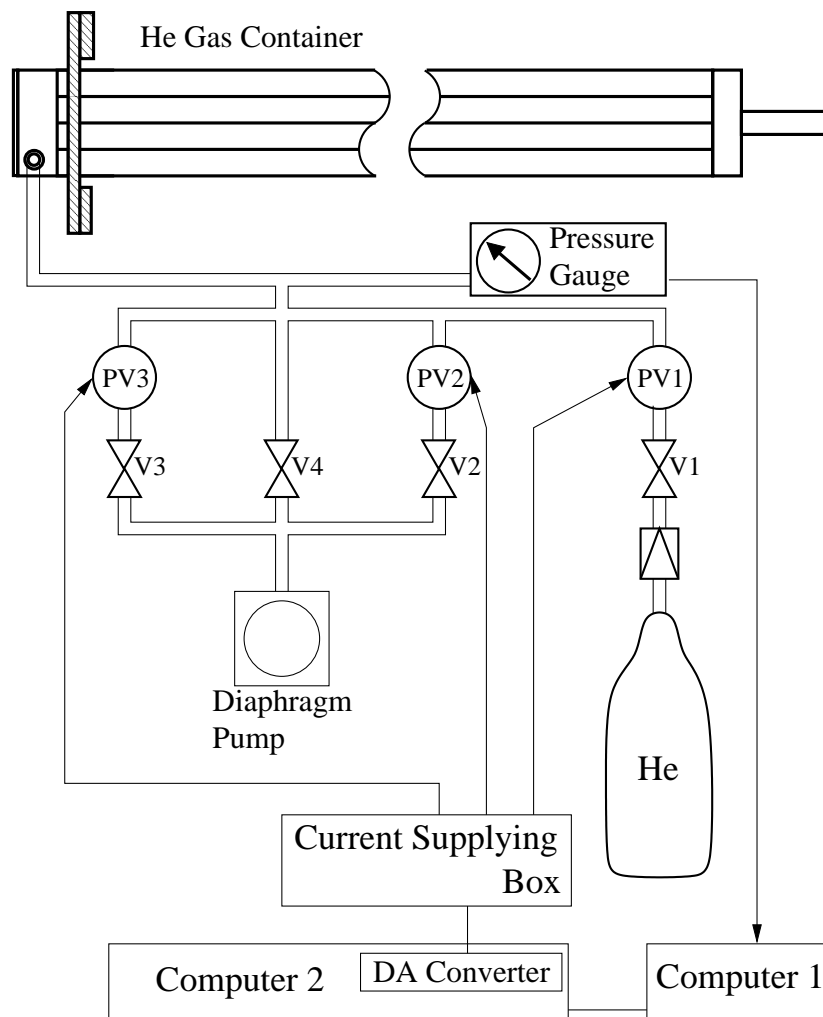


Figure 7: Diagram of pressure control system

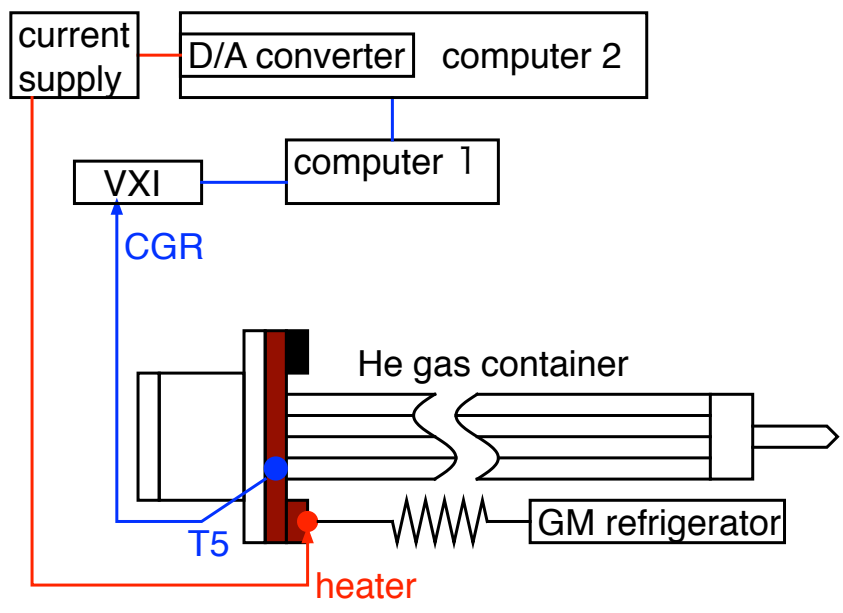


Figure 8: Diagram of temperature control system

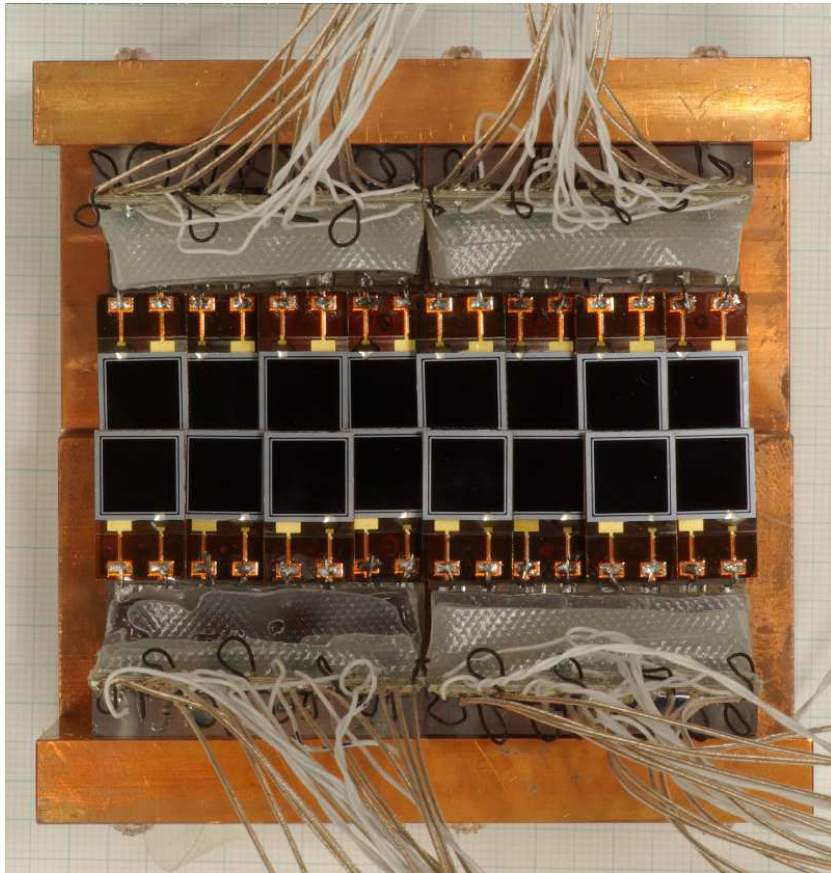


Figure 9: Photograph of PIN photodiode array

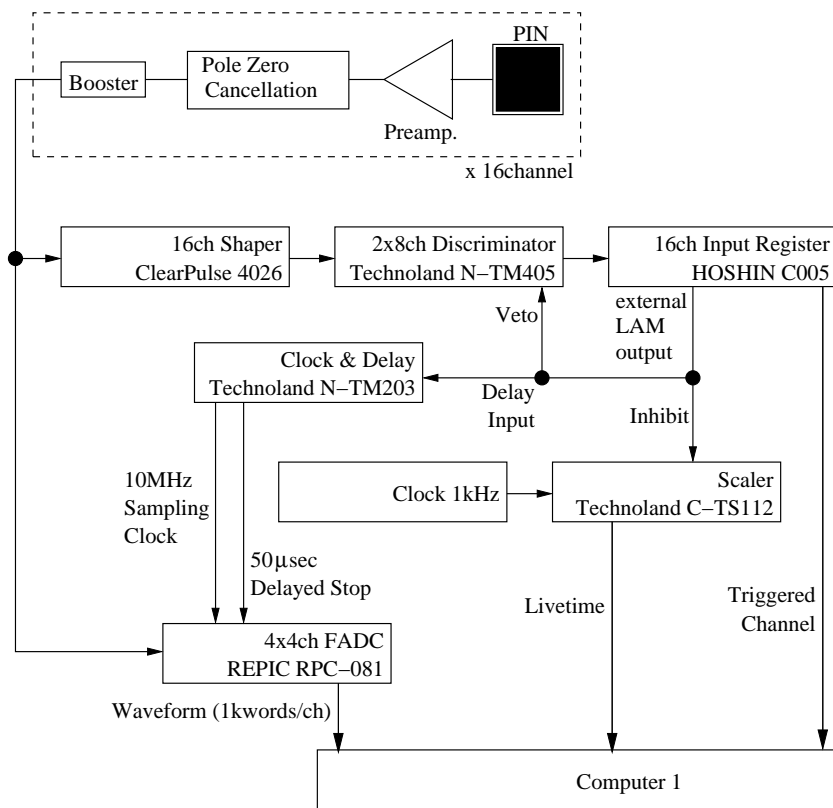


Figure 10: Diagram of DAQ system